Elastic Shear Anisotropy of Ferropericlase in Earth's Lower Mantle

Hauke Marquardt,[1]* Sergio Speziale,[1] Hans J. Reichmann,[1] Daniel J. Frost,[2] Frank R. Schilling,[1]† Edward J. Garnero[3]

Seismic shear anisotropy in the lowermost mantle most likely results from elastic shear anisotropy and lattice preferred orientation of its constituent minerals, including perovskite, post-perovskite, and ferropericlase. Measurements of the elastic shear anisotropy of single-crystal $(Mg_{0.9}Fe_{0.1})O$ up to 69 gigapascals (GPa) show that it increased considerably across the pressure-induced spin transition of iron between 40 and 60 GPa. Increasing iron content further enhances the anisotropy. This leads to at least 50% stronger elastic shear anisotropy of (Mg,Fe)O in the lowermost mantle compared to MgO, which is typically used in geodynamic modeling. Our results imply that ferropericlase is the dominant cause of seismic shear anisotropy in the lower mantle.

The lower mantle, which is dominated by an assemblage of (Mg,Fe)O ferropericlase and $(Mg,Fe,Al)(Si,Al)O_3$ perovskite [or post-perovskite (ppv) at the base of the lower mantle (*1*, *2*)], constitutes more than 50% of Earth's volume and plays a pivotal role in the evolution and present-day dynamics of our planet. Seismic shear anisotropy is a key feature within many regions of the lowermost mantle (the D″ layer) (*3*–*8*), which likely results from lattice preferred orientation (LPO) coupled with strong elastic anisotropy of lower-mantle minerals (*6*, *7*, *9*–*11*). An understanding of the mineral properties and their deformation behavior that lead to seismic anisotropy can elucidate information on mantle flow in these regions (*5*–*7*). It has been proposed that ppv (*1*, *2*) may cause seismic anisotropy in D″; however, ppv is probably a poor match to the seismic observations (*12*, *13*). It has been shown that LPO of ferropericlase leads to $V_{SH} > V_{SV}$ anisotropy (where V_{SH} and V_{SV} are the velocities of the horizontally and vertically polarized seismic shear waves, respectively) in horizontal shear (*10*); this is qualitatively consistent with seismic observations (*4*, *6*, *9*), but the contribution of (Mg,Fe)O to seismic shear anisotropy is uncertain given the small volume abundance of (Mg,Fe)O in the lower mantle (~20 vol. %).

The elastic anisotropy of ferropericlase had been determined at low pressures (*14*–*16*) or for pure MgO (*11*, *17*, *18*). In addition to the effect of Fe-Mg substitution, the spin-pairing transition of Fe^{2+} in ferropericlase (*19*) at pressures of the lower mantle affects single-crystal elastic constants (*20*), as well as bulk elastic properties (*21*–*23*). Recently, the single-crystal elastic properties of $(Mg_{0.94}Fe_{0.06})$ were measured to 60 GPa (*20*) by impulsive stimulated light scattering. That study resolved the longitudinal elastic stiffness constant c_{11}, but did not sufficiently constrain c_{12} and c_{44} (where c_{ij} are the elements of the second-order elastic stiffness tensor) for shear anisotropy to be distinguished from that of MgO.

To quantify the effect of iron content and iron spin state on the elastic shear anisotropy of (Mg,Fe)O, we performed high-pressure Brillouin scattering measurements on single-crystal $(Mg_{0.9}Fe_{0.1})O$, which was grown in a multianvil apparatus at 24 GPa and 1800°C in an Fe foil capsule (*24*) to minimize the amount of ferric iron (*25*) and associated defects. Brillouin spectroscopy was performed to 69 GPa in the diamond-anvil cell, where different pressure-transmitting media were used in different experimental runs (table S1). Information on the high-pressure density of our sample, which is needed to relate measured velocities to elastic moduli, was obtained independently from x-ray powder diffraction measurements at beamline I15 at Diamond Light Source, UK (fig. S4).

In our experiments (Fig. 1), the shear wave propagating in the [001] direction was fastest at room pressure, but its velocity remained almost constant with pressure, whereas the velocity of the shear wave along [011], polarized along [0-11], strongly increased with pressure. This led to an inversion of the fastest propagation direction at about 18 GPa. The pressure derivative of the shear wave velocity along [011] clearly increased at ~45 GPa, a pressure that corresponds to the onset of the spin transition in Fe^{2+} (*22*). The shear wave velocity along [001] was only slightly affected by the change in electronic configuration of Fe^{2+} and showed a weak depression.

The Voigt-Reuss-Hill averaged shear velocity of $(Mg_{0.9}Fe_{0.1})O$ calculated from the Brillouin data (Fig. 2) is in agreement with previous studies on (Mg,Fe)O with a variety of iron contents (*11*, *14*, *17*, *20*, *23*) that were conducted using different techniques. An increase in the mole fraction of iron causes a decrease in the average shear velocity (v_s). The pressure derivative of the shear wave velocity (dv_s/dP) decreased with increasing pressure up to ~50 GPa, where dv_s/dP steeply increased. This increase can be assigned to the spin transition of Fe^{2+} in ferropericlase, but our data do not show a clear depression in v_s associated with the spin transition, as reported in (*20*). The influence of iron on v_s becomes less pronounced once iron assumes the low-spin state.

The addition of iron increased the elastic shear anisotropy of both high-spin (HS) and low-spin (LS) (Mg,Fe)O with respect to MgO throughout the pressure regime of the lower mantle (Fig. 3). The substitution of 10% of the magnesium ions

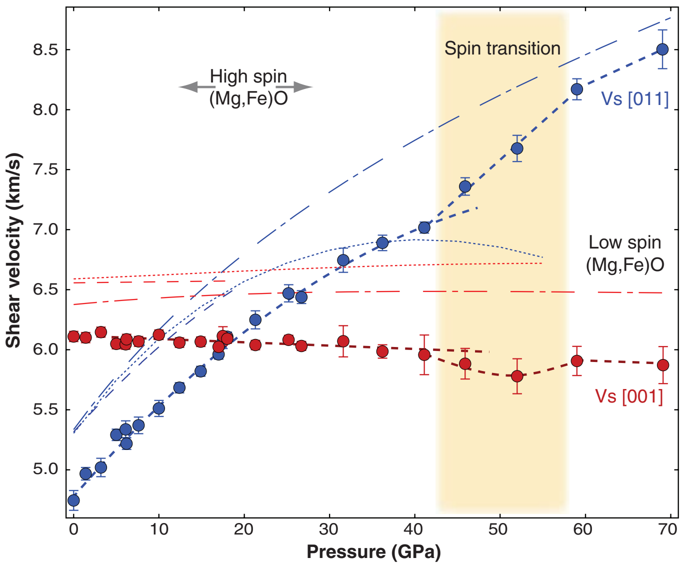

Fig. 1. Maximum and minimum shear velocities in $(Mg_{0.9}Fe_{0.1})O$ as a function of pressure. Shear velocities were measured in the (100) plane at different angles (at least seven directions) at each pressure and inverted for the two effective elastic shear constants $(c_{11} - c_{12})/2$ and c_{44}, which were used to calculate maximum and minimum shear velocity. Uncertainties are based on the propagation of the uncertainties in every measured velocity, taking into account the positions of Stokes and anti-Stokes peaks, their uncertainties, and the broadness of the peaks. The thin dashed, dotted, and dash-dotted lines are calculated from experimental (*17*, *18*) and computational (*11*) data of MgO.

[1]GFZ German Research Centre for Geosciences, Telegrafenberg, 14473 Potsdam, Germany. [2]Bayerisches Geoinstitut, Universität Bayreuth, 95440 Bayreuth, Germany. [3]School of Earth and Space Exploration, Arizona State University, Box 871404, Tempe, AZ 85287, USA.

*To whom correspondence should be addressed. E-mail: hama@gfz-potsdam.de

†Karlsruhe Institute of Technology, IBF, 76131 Karlsruhe, Germany.

Fig. 2. Increasing iron content in (Mg,Fe)O ferropericlase causes marked differences in average shear velocities. Average velocities for $(Mg_{0.9}Fe_{0.1})O$ obtained in this study by using Brillouin spectroscopy are shown as red circles. Experimental results for single-crystal MgO (*17*) (blue diamonds) and polycrystalline MgO (*32*) (blue inverse triangles), $(Mg_{0.94}Fe_{0.06})O$ (*14*, *20*) (green squares), and $(Mg_{0.75}Fe_{0.25})O$ (*23*) (yellow left-pointing triangles), along with computational data for MgO (*11*) (blue triangles), are shown for comparison.

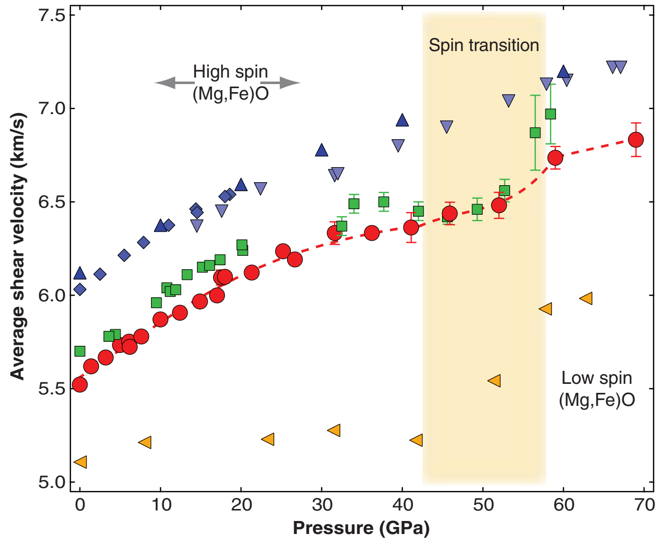

Fig. 3. Shear anisotropy of (Mg,Fe)O as a function of pressure. The shear anisotropy is defined as $(v_{s[001]} - v_{s[011]})/[(v_{s[001]} + v_{s[011]})/2]$. At pressures corresponding to those of the lower mantle, $(Mg_{0.9}Fe_{0.1})O$ (red circles) is elastically more anisotropic than iron-free MgO (blue symbols). The dashed arrow indicates that the pressure derivative of the anisotropy of ferropericlase might even be larger than for MgO; this would further increase the anisotropy difference in the lowermost mantle. Experimental data of MgO (*17*) (blue diamonds) were extrapolated (dash-dotted line) by using the pressure derivative predicted by a computational study of MgO (*11*). The only available experimental data on MgO at lower mantle pressures (*18*) (dark dotted line) show a different trend above ~20 GPa than other results, possibly caused by the limited number of measured directions (*24*). Data for $(Mg_{0.94}Fe_{0.06})O$ (*14*, *20*) (green squares) are also plotted for comparison.

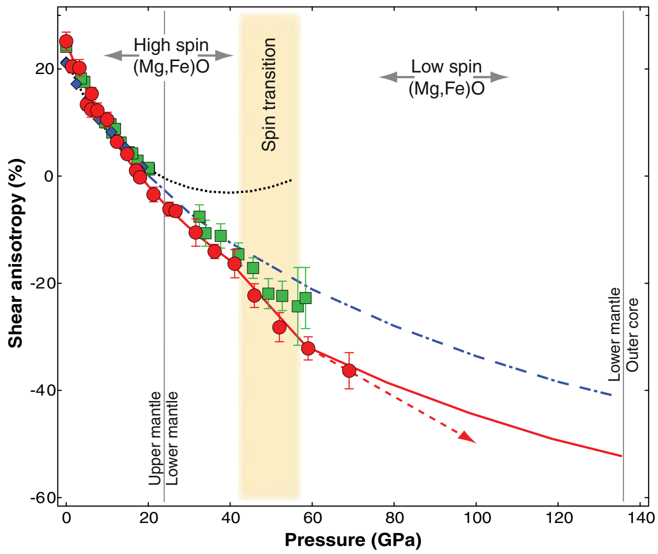

by iron not only caused an increase in anisotropy at room pressure, but also resulted in a larger pressure derivative to the anisotropy. A considerable increase in elastic shear anisotropy across the HS-LS transition was observed.

The increase in elastic anisotropy at ambient pressure cannot be explained by the size of iron (a transition metal) as in the case of alkaline-earth oxides (*26*). It can, instead, be attributed to the asymmetric electronic density distribution associated with Fe^{2+} in the HS state (*27*) that produces an increase of c_{12} (the constant that relates axial strain to orthogonal stress). The effect of pressure is to diminish the anisotropy of the 3d electron density distribution of Fe^{2+} that, combined with the negligible pressure dependence of c_{44} (Fig. 1 and fig. S2), causes a steep pressure derivative of the elastic anisotropy. With the onset of the spin transition, the 3d-electron density distribution of Fe^{2+} changes to a more symmetric configuration (*25*, *27*), causing a decrease in c_{12} and an increase of c_{11} in the LS phase.

The pressure dependence of the elastic anisotropy of LS $(Mg_{0.9}Fe_{0.1})O$ appears to be similar to that of MgO (*11*), but is shifted toward higher anisotropy (i.e., absolute value of anisotropy). This probably reflects differences in metal-oxygen bonding strength and the size difference between Mg and Fe. The difference between the elastic anisotropy of MgO and LS $(Mg_{0.9}Fe_{0.1})O$ is distinct, indicating that the HS-LS transition leads to a strong directionally dependent change in the elastic properties (Fig. 1). Assuming that the pressure dependence of the elastic anisotropy of LS $(Mg_{0.9}Fe_{0.1})O$ is identical to that of MgO, we extrapolated our data to the pressure corresponding to that of the core-mantle boundary (Fig. 3).

To evaluate the impact of our results on modeling of the elastic anisotropy of the lower mantle, we calculated the resulting maximum elastic shear anisotropy for a simplified model lower-mantle assemblage of ~80 vol. % $MgSiO_3$ and ~20 vol. % $(Mg_{0.8}Fe_{0.2})O$ (*24*). Our results show that the elastic shear anisotropy of (Mg,Fe)O strongly depends on the iron content and that ~20

Fig. 4. Maximum shear anisotropy of major lower-mantle phases along a model geotherm. The shear polarization anisotropy is defined as $(v_{s,max} - v_{s,min})/[(v_{s,max} + v_{s,min})/2]$, where $v_{s,max}$ and $v_{s,min}$ are maximum and minimum shear velocity in a given direction. (**A**) The maximum single-crystal polarization anisotropy of the two major components of Earth's lower mantle. The shear anisotropy of MgO (gold) and $MgSiO_3$ (blue) were calculated with available computational data at high pressure and temperature. The elastic anisotropy of $(Mg_{0.8}Fe_{0.2})O$ (red), a model mantle composition, was linearly scaled from the data of MgO and $(Mg_{0.9}Fe_{0.1})O$, corrected for temperature (*24*). The expected broadening of the spin transition region (dashed lines) with temperature was estimated from experimental data on $(Mg_{0.75}Fe_{0.25})O$ (*33*). (**B**) The anisotropies of the single phases were weighted by their volume abundance in the lower mantle (*24*), where the shaded areas illustrate the maximum possible contributions of perovskite (blue) and ferropericlase (red), a situation in which all the crystals of the same mineral phase have the same orientation.

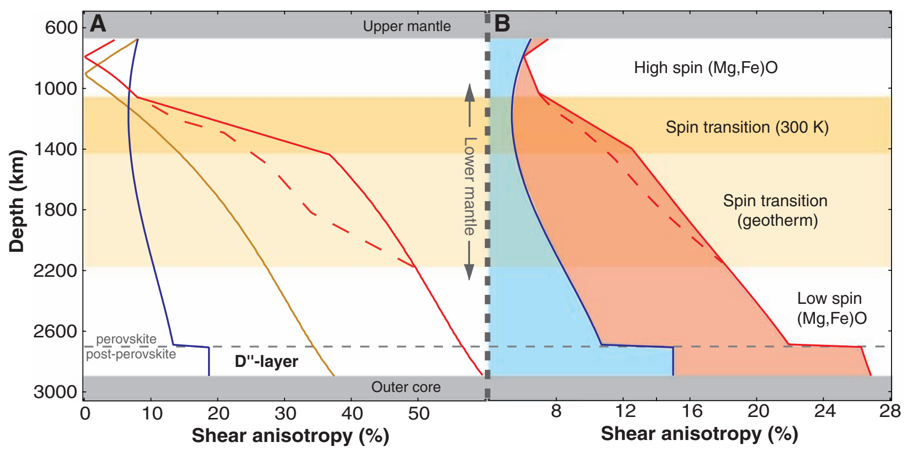

vol. % of $(Mg_{0.8}Fe_{0.2})O$ contribute about equally to the overall possible seismic shear anisotropy as ~80 vol. % $MgSiO_3$ (Fig. 4). Because (Mg,Fe)O is a much weaker phase (*28*), it will accommodate most of the strain (*29*); it should, therefore, develop a much stronger texture than $(Mg,Fe)SiO_3$ (*13*). Thus, it is likely that LPO of (Mg,Fe)O dominates seismic anisotropy in the lower mantle. Strong partitioning of iron into ferropericlase, suggested by experiments (*19*, *30*), may favor even stronger anisotropy from (Mg,Fe)O. However, consensus on the partitioning behavior of iron under lower-mantle conditions has not been reached (*30*, *31*).

If LPO of ferropericlase dominates lower-mantle anisotropy, seismic anisotropy could also be present above the D″ discontinuity in regions where deformation is dominated by dislocation creep at very high strain levels (*6*, *9*). The rapid spreading of seismic receivers around the world will allow us to better quantify the depth distribution of anisotropy in the lower mantle.

References and Notes

1. M. Murakami, K. Hirose, K. Kawamura, N. Sata, Y. Ohishi, *Science* **304**, 855 (2004).
2. A. R. Oganov, S. Ono, *Nature* **430**, 445 (2004).
3. T. Lay, Q. Williams, E. J. Garnero, *Nature* **392**, 461 (1998).
4. E. J. Garnero, V. Maupin, T. Lay, M. J. Fouch, *Science* **306**, 259 (2004).
5. M. Panning, B. Romanowicz, *Science* **303**, 351 (2004).
6. A. K. McNamara, P. E. van Keken, S.-I. Karato, *Nature* **416**, 310 (2002).
7. J. Wookey, S. Stackhouse, J. M. Kendall, J. Brodholt, G. D. Price, *Nature* **438**, 1004 (2005).
8. J. M. Kendall, P. G. Silver, *Nature* **381**, 409 (1996).
9. H. R. Wenk, S. Speziale, A. K. McNamara, E. J. Garnero, *Earth Planet. Sci. Lett.* **245**, 302 (2006).
10. D. Yamazaki, S.-i. Karato, *Phys. Earth Planet. Inter.* **131**, 251 (2002).
11. B. B. Karki, R. M. Wentzcovitch, S. de Gironcoli, S. Baroni, *Science* **286**, 1705 (1999).
12. S. Merkel *et al.*, *Science* **316**, 1729 (2007).
13. R. M. Wentzcovitch, T. Tsuchiya, J. Tsuchiya, *Proc. Natl. Acad. Sci. U.S.A.* **103**, 543 (2006).
14. J. M. Jackson *et al.*, *J. Geophys. Res.* **111**, B09203 (2006).
15. S. D. Jacobsen *et al.*, *J. Geophys. Res.* **107**, 2037 (2002).
16. H. J. Reichmann, S. V. Sinogeikin, J. D. Bass, *Am. Mineral.* **93**, 1306 (2008).
17. S. V. Sinogeikin, J. D. Bass, *Phys Earth Planet. Inter.* **120**, 43 (2000).
18. C.-S. Zha, H.-k. Mao, R. J. Hemley, *Proc. Natl. Acad. Sci. U.S.A.* **97**, 13494 (2000).
19. J. Badro *et al.*, *Science* **300**, 789 (2003).
20. J. C. Crowhurst, J. M. Brown, A. F. Goncharov, S. D. Jacobsen, *Science* **319**, 451 (2008).
21. J.-F. Lin *et al.*, *Nature* **436**, 377 (2005).
22. S. Speziale *et al.*, *Proc. Natl. Acad. Sci. U.S.A.* **102**, 17918 (2005).
23. J.-F. Lin *et al.*, *Geophys. Res. Lett.* **33**, L22304 (2006).
24. Materials and methods are available as supporting material on *Science* online.
25. H. Keppler, I. Kantor, L. Dubrovinsky, *Am. Mineral.* **92**, 433 (2007).
26. T. Tsuchiya, K. Kawamura, *J. Chem. Phys.* **114**, 10086 (2001).
27. T. Tsuchiya, R. M. Wentzcovitch, C. R. S. da Silva, S. de Gironcoli, *Phys. Rev. Lett.* **96**, 198501 (2006).
28. S.-i. Karato, *Phys Earth Planet. Inter.* **55**, 234 (1989).
29. K. Madi, S. Forest, P. Cordier, M. Boussuge, *Earth Planet. Sci. Lett.* **237**, 223 (2005).
30. M. Murakami, K. Hirose, N. Sata, Y. Ohishi, *Geophys. Res. Lett.* **32**, L03304 (2005).
31. Y. Kobayashi *et al.*, *Geophys. Res. Lett.* **32**, L19301 (2005).
32. M. Murakami, Y. Ohishi, N. Hirao, K. Hirose, *Earth Planet. Sci. Lett.* **277**, 123 (2009).
33. J.-F. Lin *et al.*, *Science* **317**, 1740 (2007).

34. We thank J.-F. Lin, S. Jahn, T. Duffy, M. Koch-Müller, R. Jeanloz, K. Hartmann, and two anonymous reviewers for helpful comments and ideas on the project and the manuscript; A. Kurnosov for gas-loading at Bayerisches Geoinstitut, H. Wilhelm for assistance at the Diamond Light Source; and M. Gottschalk and T. Boffa Ballaran for single-crystal x-ray diffraction. E.J.G. acknowledges support from NSF grant EAR-0711401.

Supporting Online Material

www.sciencemag.org/cgi/content/full/324/5924/224/DC1
Materials and Methods
Figs. S1 to S5
Table S1
References

4 December 2008; accepted 16 February 2009
10.1126/science.1169365

A Great Earthquake Rupture Across a Rapidly Evolving Three-Plate Boundary

Kevin P. Furlong,[1]* Thorne Lay,[2] Charles J. Ammon[1]

On 1 April 2007 a great, tsunamigenic earthquake (moment magnitude 8.1) ruptured the Solomon Islands subduction zone at the triple junction where the Australia and Solomon Sea–Woodlark Basin plates simultaneously underthrust the Pacific plate with different slip directions. The associated abrupt change in slip direction during the great earthquake drove convergent anelastic deformation of the upper Pacific plate, which generated localized uplift in the forearc above the subducting Simbo fault, potentially amplifying local tsunami amplitude. Elastic deformation during the seismic cycle appears to be primarily accommodated by the overriding Pacific forearc. This earthquake demonstrates the seismogenic potential of extremely young subducting oceanic lithosphere, the ability of ruptures to traverse substantial geologic boundaries, and the consequences of complex coseismic slip for uplift and tsunamigenesis.

Great earthquakes typically involve sudden sliding between two tectonic plates, and the largest events are located in subduction zones where an oceanic plate thrusts into the mantle below an overriding plate. In a few locations, a boundary between two oceanic plates impinges on a subduction zone, causing both plates to descend beneath the overriding plate, but at different rates and directions. This is the situation that led to the great moment magnitude M_w 8.1 Solomon Islands earthquake of 1 April 2007 [8.47°S, 157.04°E, 20:39:58.7 UTC (*1*)], which ruptured the megathrust between the overriding Pacific plate (PaP) and the independently subducting Australia (AuP) and Solomon Sea–Woodlark Basin (SWP) plates (Fig. 1). The inferred rupture area along the San Cristobal and New Britain trenches, as indicated by aftershocks (*1*), patterns of uplift/subsidence (*2*–*4*), and preliminary rupture analysis (*5*, *6*), straddles the down-dip extension of the Simbo transform fault that separates the SWP from the AuP; thus, the earthquake ruptured across the SWP-AuP plate boundary. The rupture generated a large local tsunami, and about 50 lives were lost and more than 9000 people displaced.

[1]Department of Geosciences, The Pennsylvania State University, State College, PA 16802 USA. [2]Department of Earth and Planetary Sciences, University of California, Santa Cruz, CA 95064, USA.

*To whom correspondence should be addressed. E-mail: kevin@geodyn.psu.edu

Before the 2007 event, this triple junction region, where the three plates meet, had low seismic activity and no record of large interplate events (*7*); thus, pre-event seismicity, or other available geologic and tectonic data, provided limited constraint on the subduction zone geometry. The region above the down-dip extension of the Simbo Fault is a localized region of rapid Holocene uplift (*8*). The age of lithosphere currently subducting along the trench varies from ~0.5 to 3.5 million years old, and it has been speculated that such young, hot lithosphere will not produce large earthquakes. Here we describe the 2007 earthquake rupture to address how, before the earthquake, strain was distributed between the subducting and overriding plates.

Before ~0.5 million years ago (Ma), the easternmost segment of the Woodlark Basin spreading ridge was subducting beneath the western margin of the Solomon Islands (Fig. 1), and the ridge-trench triple junction migrated northwesterly at ~110 to 120 mm/year. The differences in plate subduction rates and directions produced a slab window, which today lies beneath the southern New Georgia Islands. The SWP subducts at 135 mm/year (N45°E), whereas the AuP subducts at 97 mm/year (N70°E) (*8*, *9*). The near-total cessation of spreading on the most trenchward section of the Woodlark Basin ridge at ~0.5 Ma (*8*, *9*) and the formation of the right-lateral

Science

Elastic Shear Anisotropy of Ferropericlase in Earth's Lower Mantle

Hauke Marquardt, Sergio Speziale, Hans J. Reichmann, Daniel J. Frost, Frank R. Schilling and Edward J. Garnero

Science **324** (5924), 224-226.
DOI: 10.1126/science.1169365

Science (print ISSN 0036-8075; online ISSN 1095-9203) is published by the American Association for the Advancement of Science, 1200 New York Avenue NW, Washington, DC 20005. The title *Science* is a registered trademark of AAAS.

American Association for the Advancement of Science